Investigation of the Amorphous to Crystalline Transition in Indium Tin Oxide Films

Colleen Nehl
Office of Science, Energy Research Undergraduate
Laboratory Fellowships (ERULF)
University of California, Santa Barbara
National Renewable Energy Laboratory
Golden, Colorado

August 23, 2000

Prepared in partial fulfillment of the requirements of the Office of Science, Department of Energy, Energy Research Undergraduate Laboratory Fellowships under the direction of Dr. David Ginley in the Solar Energy Research Facility at the National Renewable Energy Laboratory.

Participant: _____
Signature

Research Advisor: _____
Signature

Table of Contents

Abstract

Investigation of the Amorphous to Crystalline Transition in Indium Tin Oxide. Colleen Nehl (University of California, Santa Barbara, Santa Barbara, CA, 93107) David Ginley (National Renewable Energy Laboratory, Golden, Colorado 80401).

Transparant conducting oxides (TCO's) are needed for applications like solar cells. These TCO's, may be able to be optimized by understanding the amorphous to crystalline transition in TCO's. We investigated this transition and the change in relevant electro-optical properties by using indium tin oxide (ITO) deposited at different temperatures and amounts of oxygen, and then annealing it to induce the change from amorphous to crystalline. Our investigation revealed that resistivity usually decreases as crystallinity increases. We also saw slight increases in transparency with annealing. This research may offer new information about the crystallization mechanism for ITO, and possibly other TCOs. Understanding this amorphous to crystalline transition may, with further research, allow us to understand how to optimize electro-optical properties for current and future TCO applications.

Research Category (Please Circle)

ERULF: **Physics**	Chemistry	Biology	Engineering	Computer Science	Other
CCI: Biotechnology	Environmental Science		Computing		

TYPE ALL INFORMATION CORRECTLY AND COMPLETELY

School Author Attends:		University of California, Santa Barbara
DOE National Laboratory Attended:		National Renewable Energy Laboratory
Mentor's	Name:	Dr. David Ginley
	Phone:	(303) 384-6573
	E-mail :	David_Ginley@nrel.gov

Author's Name:	Colleen Nehl
Mailing Address:	11539 Judy St.
City/State/ZIP	Maryville, CA 95901
Phone:	(530) 743-6050
E-mail Address:	cnehl@umail.ucsb.edu

Is this being submitted for publication?: Yes No

DOE Program: **ERULF** CCI PST (circle one only)

Introduction

Imagine a world where energy efficient window coatings and new solar cells help us to save energy, save resources, and save our planet. At the National Renewable Energy Laboratory, we're researching materials that can help make this future possible. Indium Tin Oxide is already a key part of solar cells, window coatings, energy efficient buildings, and flat panel displays (Xirouchaki, June 1996). Learning more about Indium Tin Oxide, or ITO, has tremendous potential to improve these products. In solar cells, for example, ITO can be the transparent, conducting top layer that lets light shine into the cell, and electricity flow out. Improving the ITO layer can help improve the solar cell efficiency.

A transparent conducting oxide is a material with high transparency in a derived part of the spectrum and high electrical conductivity. Beyond these key properties of TCOs (transparent conducting oxides), ITO has a number of other key characteristics. Internal structure can be amorphous, crystalline, or mixed, depending on the deposition temperature and atmosphere. In general, ITO deposited at room temperature is amorphous, and ITO deposited at higher temperatures is crystalline. Depositing at high temperatures is more expensive than at room temperature, and this method may not be compatible with the underlying devices. Unfortunately, the electro-optical properties are a function of the crystallinity of the material. The research reported here points to a possible new way of making optimum ITO films through depositing at room temperature and then annealing.

A key point from this work is that it is not always essential to have purely crystalline TCOs (transparent conducting oxides), because partially-amorphous samples can perform as well—perhaps even better—than crystalline. In other words, there's a range of performance between purely amorphous and purely crystalline. Optimum performance for a particular

application could be anywhere in this range. Somewhere during the amorphous to crystalline transition we may find the material that'll optimize transparency and conductivity for current and future applications. By understanding more about this transition, we may be able use deposition temperature, amount of oxygen present at deposition, and the annealing temperature to design the right TCO for a particular application. Our research may also be applicable to other TCOs, an important point because there are some questions about the worldwide availability of indium. We'll also have greater understanding of and control over which wavelengths of light (visible, infrared, ultraviolet) shine through ITO, a key feature in energy efficient windows and in solar cells.

So, to explain what was done in this research, we'll first look at the characterization methods used. Characterization methods are the methods used to investigate structural and electro-optical properties of ITO through laboratory testing. We had one major goal in this research: to understand the relationship between structural and electro-optical changes in ITO. To understand structural changes, x-ray diffraction and Raman spectroscopy were employed. Data on electro-optical properties was provided by UV-Vis-NIR (ultraviolet, visible, near infrared spectroscopy), FTIR (Fourier transform infra-red spectroscopy), and the Hall system.

To explain this research and its implications, we'll first look at the experimental methodology used. Next, we'll discuss the specifics of the experiments and turn our attention to the results. Finally, we'll examine our results and consider future directions for ITO and TCO research and applications.

Experimental Methodology

The procedure for this investigation involved annealing the samples and then characterizing them. Annealing means heating a sample for a period of time with the intent to

cause a change in the material. Characterization is the use of laboratory testing to explore key properties. Now that our methodology is clear, let's consider our samples, experiments, and characterization methods.

Samples

Electron beam sputtering and DC sputtering were used to produce samples. David Paine of Brown University provided e-beam (electron beam) and DC sputtered samples on glass. Films are 100-120 nm thick. Samples on PET (polyethylene terpthalate, a flexible polymer) are from Pacific Northwest Laboratory. A table of specific deposition conditions and parameters is in Table 1.

Experimental Procedure

In our investigation, we had six different samples of ITO, deposited under different conditions onto different substrates. Four of the six samples were deposited on glass. Samples on glass were divided into nine pieces. Six of the nine pieces were annealed in air at 50°, 100°, 150°, 200°, 250°, or 300° C and then characterized. One piece of each was set aside as a room temperature control and two were set aside as backups. The samples on PET were divided into 3-4 pieces. For the PET samples, one piece served as a control, one was annealed at 50° C, one at 200° C, and for the sample with four pieces, one at 100°C. After annealing, samples were characterized.

Every sample had its key parameters measured at room temperature and following annealing. Following every annealing session, data went in a matrix like the one in Table 2. After the anneals and their characterizations were carried out, we can form a second experimental matrix (Table 3) with properties as a function of annealing temperature. One matrix

is formed for every key property explored. Tables and graphs for the data in the matrices are in the Tables and Figures section at the end of this paper.

Characterization:

XRD (X-Ray Diffraction)

XRD gives us information about the long-range order inside the substance. A Scintag X1 Advanced Diffraction System was used for these measurements. Peaks on the graphs in figures 1-6 correspond to crystalline phases. The stronger a peak, the more of the phase is present. If there are no peaks, then the material is amorphous on the large scale. The 'hump' on the graphs between approximately 20° and 35° is due to the glass substrate. See figure 7 for the XRD scan of the glass substrate.

Raman Spectroscopy

Raman gives information on the short-range order in a substance. We tried Raman on several samples, but the analysis provided no useful data. We suspect that our samples were too conductive for Raman spectroscopy to be a useful method of characterization.

UV-Vis-NIR and FTIR (ultraviolet, visible, near infra red, and Fourier transform infra-red spectrophotometer analysis)

A desktop Ocean Optics CCD Based Spectrophotometer provided information on the transparency in the visible and UV range and on the band-gap of our samples. A Nicolet system was used for Fourier transform infra-red spectroscopy. It provided information on reflectivity in the infra red range, as well as the band gap.

Hall Measurements

Provided information about resistivity, carrier concentration and mobility. Used a BioRad HL5500 Hall System. Indium solder was used for contacts.

Results:

In general, crystallinity increased with annealing. For all amorphous samples there was no evidence of crystallinity until annealed to at least 100° C. Some samples had no crystalline peaks until annealing at 200° C. From 200° C-300° C, annealing increased crystallinity. For samples that were already crystalline, annealing at all temperatures increased their crystallinity slightly.

Crystalline samples also have, as expected, a lower resistivity than amorphous samples. As crystallinity increases, resistivity decreases. One notable exception is discussed in the Hall measurement section of the discussion.

XRD

Structurally, X-ray diffraction revealed that after initial crystallization our samples became more crystalline with each anneal, as stated before. Figures 1-6 show this change. Peaks at 30.58°, 35.47°, 51.04°, and 60.68°, reveal InO_2 (PDF 6-416). A noteworthy feature is the peak at 44.12° degrees present on all samples after the 200°-degree anneal. It nearly matches the 101 peak at 44.6° degrees of $InSn_4$, a metallic alloy (PDF 7-396). No other peaks matching $InSn_4$ are present. And its presence would be surprising. This peak is, at present, a mystery.

Raman Spectroscopy

We suspect that the samples were too conductive, so Raman yielded no meaningful data.

UV-Vis-NIR/FTIR

Our DC sputtered samples were very transparent in the visible range, and had an average transparency of 80% between 350 and 950 nm. Transparency increased slightly with annealing, as seen in figures 9-12, but the increases were well within the uncertainty of the desktop spectrophotometer.

For our electron-beam deposited sample (E-Beam), between the as-deposited sample and the sample annealed at 300° C, transparency increased between 3x and 10x in the region of 350-950 nm. Interestingly enough, much of this increase was during the annealing at 250° C and the annealing at 300° C. For the sample deposited at 350° C, annealing did not significantly increase the region of high transparency. The samples deposited by DC sputtering at room temperature exhibited a slight increase in transparency in the region 380 nm to 330 nm. These two samples differ in the amount of oxygen present at deposition. See table 1. Figures 10-11 show the increase in transparency.

Hall Measurements

Resistivity is nearly constant for crystalline samples and near-crystalline samples. For amorphous samples, resistivity decreases dramatically—at least 2 orders of magnitude. The 'exception' to this is the behavior of the DC N-3 sample deposited by sputtering at room temperature in 10% oxygen. Resistivity increases sharply before it decreases. Graph 8 illustrates this.

Discussion of Results

XRD

The formation of InO_2 peaks was expected, and consistent with the work of Paine et al. as well as the work of Wulff, Quaas, and Steffen, all in 1999. These author's regions of investigation extended from 20° to 40° (Paine 1999), and 25° to 40° (Wulff et al. 1999). Since the scans I performed for this experiment ranged from 5°-90°, we had more information to work with. This also means that we can confirm some of our results by comparisons with these papers. The presence of the 30.58° degree and 35.47° degree peaks was expected and consistent with the papers cited above. For the unidentified peak at 44.12° degrees, we can gain no outside

information from these papers. We speculate that this peak may be due to contamination of the sample, or anomalous XRD set up. Another important point is that the peak has 'disappeared.' It was present on the day of the first XRD scan, but now is not. Two weeks after the first scan we did another XRD scan of the region, and did not locate the peak again. We tried to recreate this peak by annealing a sample at 200° C for 6 hours, and doing XRD immediately after annealing. No peak was detected. Later annealing (at 250° C and 300° C did not produce a peak either.

Raman Spectroscopy

As we gathered no useful Raman data, we have no results to discuss.

UV-Vis-NIR/FTIR

Transparency did increase, in general, for the samples. On some samples, we may also be seeing a slight movement of the band gap. But the movement is slight, difficult to see (see graphs 9-12), and possibly within the uncertainty of the instrument used. Further research, namely transparency data taken under carefully controlled conditions would be appropriate to investigate this further.

Hall Measurements

As expected, resistivity decreased with crystallinity. See figures 1-10 for crystallinity increases. Figure 9 shows resistivity as a function of annealing temperature. The decrease of resistivity was not linear, and it featured numerous irregularities. Looking to the behavior of the sample deposited at room temperature and 10% O2 (DC N-3), we see that before resistivity drops, it increases by an order of magnitude. This was unexpected, and further research may be able to identify the cause of this increase and drop. Information about the crystallization mechanism may also be provided from this data. A possible hypothesis for this phenomenon is that as the sample begins to crystallize, it has many, very small crystalline regions. Each

crystalline region has a grain boundary. So as the sample crystallizes further, there are more and more small regions of crystallinity, and more and more of the sample is taken up in the grain boundary. As the crystallinity grows the sample is dominated by the grain boundary, which raises the resistivity. Once the small regions of crystallinity begin to grow together, less of the sample may be grain boundary, so the resistivity could drop.

Discussion and Conclusion

This research serves as a confirmation of what we suspected, and opens the door for further research and improvements in ITO, and possibly general TCO applications. First, we've seen confirmation of the expected in that resistivity does, in general, decrease with annealing. And that resistivity does, in general, decrease as crystallinity increases. Further research on the exception to this (as discussed in the XRD discussion of results); may provide new information on the relationship between crystallinity and resistivity, as well as the crystallization mechanism for ITO, and possibly other TCOs.

Acknowledgements

I'd like to thank my mentor, Dr. David Ginley, for directing me in this research. Also thanks to John Perkins for the FTIR data, Raman data, excellent explanations, and guidance in this project. Thanks to Phil Parilla for encouragement, explanations, and help with the XRD data. Also thanks to Tim Gessert for help with the Hall, and Tayna Rivkin for the Compound Light Microscope pictures, as well as to David Paine of Brown University for the samples.

Thanks also to the National Renewable Energy Laboratory, ERULF (Energy Research Undergraduate Laboratory Fellowships), as well as the U.S. Department of Energy for this opportunity. Also to Linda Lung for organizing this.

The research described in this paper was performed at the Solar Energy Research Facility at the National Renewable Energy laboratory, as sponsored by the U.S. Department of Energy—Office of Science, ERULF program.

References:

Asbalter, J. & Subrahmanyam, A. (2000). "P-type transparent conducting In2O3-Ag2O thin films prepared by reactive electron beam evaporation technique" Journal of Vacuum Science Technology. 18(4),. pp 1-5.

Coutts, T.J., Gessert, T.A., Dhere, R.G., Nelson, A.J. & Aharoni H. (1986). "Ion Beam Sputtered ITO As a Window Layer Material for Photovoltaic Applications." Rev. Brasil. Apl. Vacuum, 6,. pp 289-317.

Gao, Z., Gao, Y., Li, Yonghong & Li, Yi. "Effects of Heat Treatment on the Microstructure of Nanophase Indium-Tin Oxide." NanoStructured Materials. 11 (5). pp 611-616.

Morikawa, H. & Fujita, M., (1999). "Crystallization and decrease in resistivity on heat treatment of amorphous indium tin oxide thin fioms prepared by d.c. magnetron sputtering." Thin Solid Films, 339,. pp 309-313.

Morikawa, H. & Fujita, M., (2000). "Crystallization and electrical property change on the annealing of amorphous indium-oxide and indium-tin-oxide thin films." Thin Solid Films, 359,. pp 61-67.

Paine, D. C., Whitson, T., Janiac, D., Beresford, R., Yang, C. O. & Lewis, B. "A study of low temperature crystallization of amorphous thin film indium-tin oxide." Journal of Applied Physics. 85 (12). pp 8445-8450.

Quaas, M., Steffen, H. & Wulff, H. "GIXR and GIXRD Investigations of ITO Films during Post-Deposition Annealing." Materials Science Forum. 321-324. pp 434-438.

Wulff, H., Quaas, M. & Steffen, H. (1999). "Investigation of plasma-deposited ITO films by GIXR and GIXRD" Thin Solid Films, 355-356,. pp 395-400.

Xirouchaki, C., Kiriakids, G., Pedersen T.F. & Fritzsche, H. (1996) "Photoreduction and oxidation of as-deposited microcrystalline indium oxide." Journal of Applied Physics, 79 (12),. pp 9349-9352.

Tables

	Sputtering Temperature	% O_2 Present	Method	Substrate
DC N-1	350° C	0.08%	DC	Glass
DC N-2	Room Temp	0.08%	DC	Glass
DC N-3	Room Temp	10%	DC	Glass
EB N-1	Room Temp		E-Beam	Glass
PET A				PET (polyethylene terpthalate, a flexible polymer)
PET B				PET

Table 1 above. Shows deposition conditions and substrate information for samples

	Key Parameters
Sample 1	
Sample 2	
Sample 3	
Sample 4	
Sample 5	

Table 2 above. Experimental Matrix.

	RT	**50° C**	**100°C**	**150°C**	**200°C**	**250°C**	**300°C**
Sample 1							
Sample 2							
Sample 3							
Sample 4							
Sample 5							

Table 3 above. Properties as a function of annealing temperature

	RT	**50° C**	**100°C**	**150°C**	**200°C**	**250°C**	**300°C**
Sheet Resistivity for 350°C/	32	22	31.3	21.1	28.6	38.2	48.2

0.08% O_2 Sheet Resistivity for Room Temp/0.08% 0_2	31.7	28.3	31	34.1	83.6	57.9	55.2
Sheet Resistivity for Room Temp/10% 0_2	3800	6320	39800	32100	5170	342	273
Sheet Resistivity for Electron-beam deposited	2520	2650	2780	34.5	15.3	19.1	28

Table 4 above. Sheet resistivity as a function of annealing temperature. See Figure 12 for more information. All values are in Ohms/square.

Figures

Tables

	Sputtering Temperature	% O_2 Present	Method	Substrate
DC N-1	350° C	0.08%	DC	Glass
DC N-2	Room Temp	0.08%	DC	Glass
DC N-3	Room Temp	10%	DC	Glass
EB N-1	Room Temp		E-Beam	Glass
PET A				PET (polyethylene terpthalate, a flexible polymer)
PET B				PET

Table 1 above. Shows deposition conditions and substrate information for samples

	Key Parameters
Sample 1	
Sample 2	
Sample 3	
Sample 4	
Sample 5	

Table 2 above. Experimental Matrix.

	RT	**50° C**	**100°C**	**150°C**	**200°C**	**250°C**	**300°C**
Sample 1							
Sample 2							
Sample 3							
Sample 4							
Sample 5							

Table 3 above. Properties as a function of annealing temperature

	RT	**50° C**	**100°C**	**150°C**	**200°C**	**250°C**	**300°C**

Sheet Resistivity for 350°C/ 0.08% O_2	32	22	31.3	21.1	28.6	38.2	48.2
Sheet Resistivity for Room Temp/0.08% 0_2	31.7	28.3	31	34.1	83.6	57.9	55.2
Sheet Resistivity for Room Temp/10% 0_2	3800	6320	39800	32100	5170	342	273
Sheet Resistivity for Electron-beam deposited	2520	2650	2780	34.5	15.3	19.1	28

Table 4 above. Sheet resistivity as a function of annealing temperature. See Figure 12 for more information. All values are in Ohms/square.

Figures

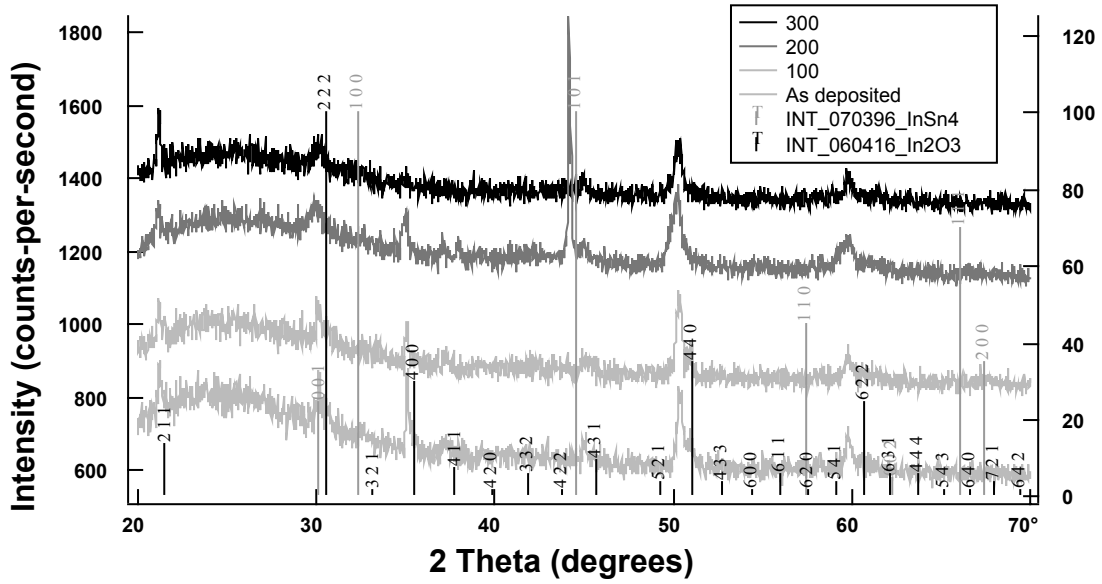

Figure 1 above. Shows x-ray diffraction data for scans of sample DC N-1 (350° C/0.08% O2) after annealing in increments of 100° C. PDF traces are 7-396 ($InSn_4$) and 6-416 (In_2O_3).

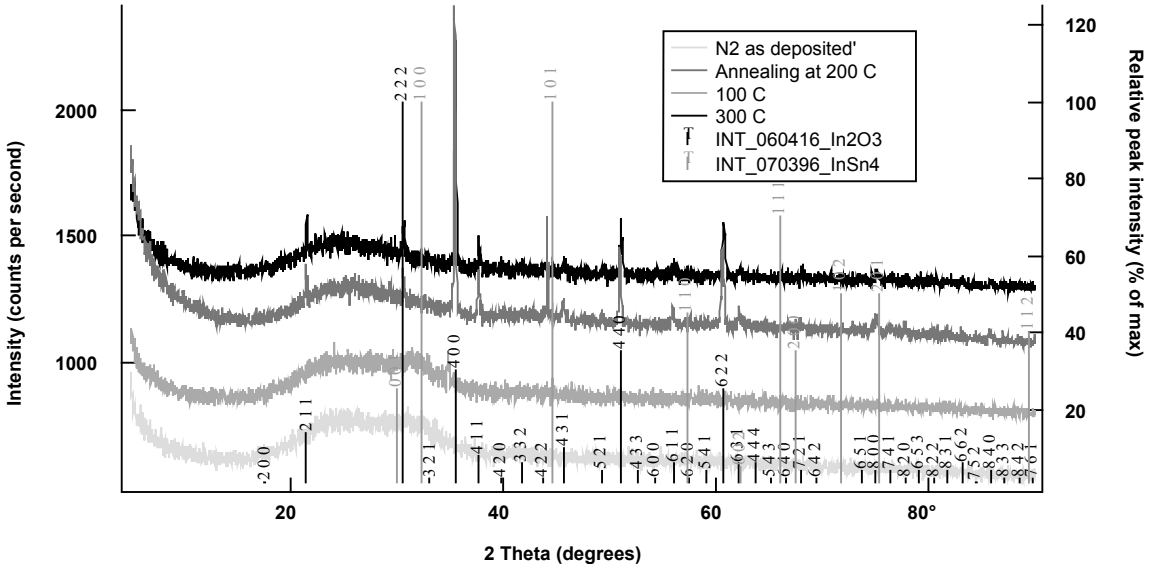

Figure 2 above. Shows x-ray diffraction data for scans of sample DC N-2 (room temperature/0.08% O2) after annealing in increments of 100° C. PDF traces are 7-396 ($InSn_4$) and 6-416 (In_2O_3).

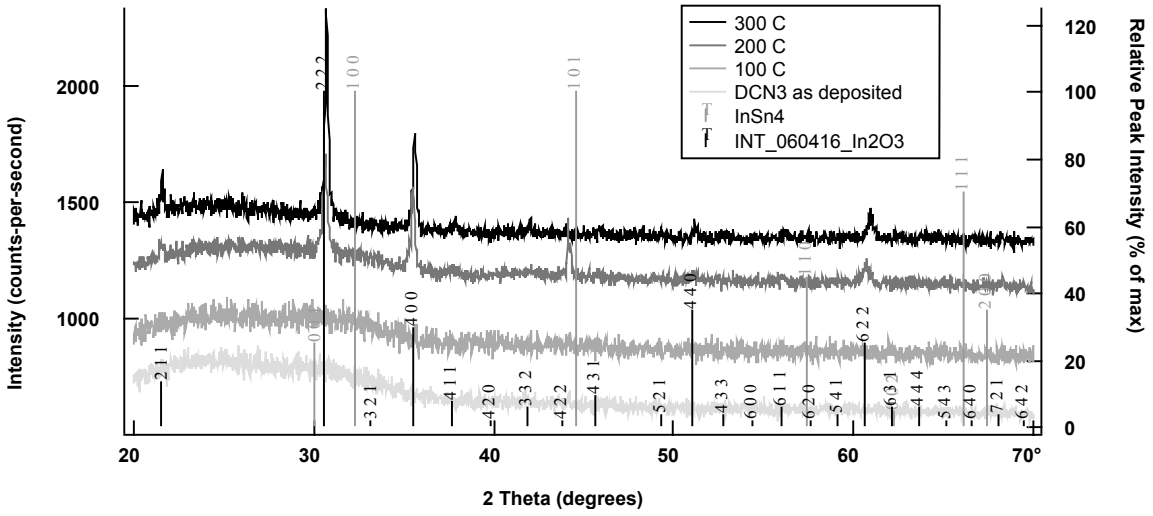

Figure 3 above. Shows x-ray diffraction data for scans of sample DC N-3 (room temperature/ 10% O2) after annealing in increments of 100° C. PDF traces are 7-396 ($InSn_4$) and 6-416 (In_2O_3).

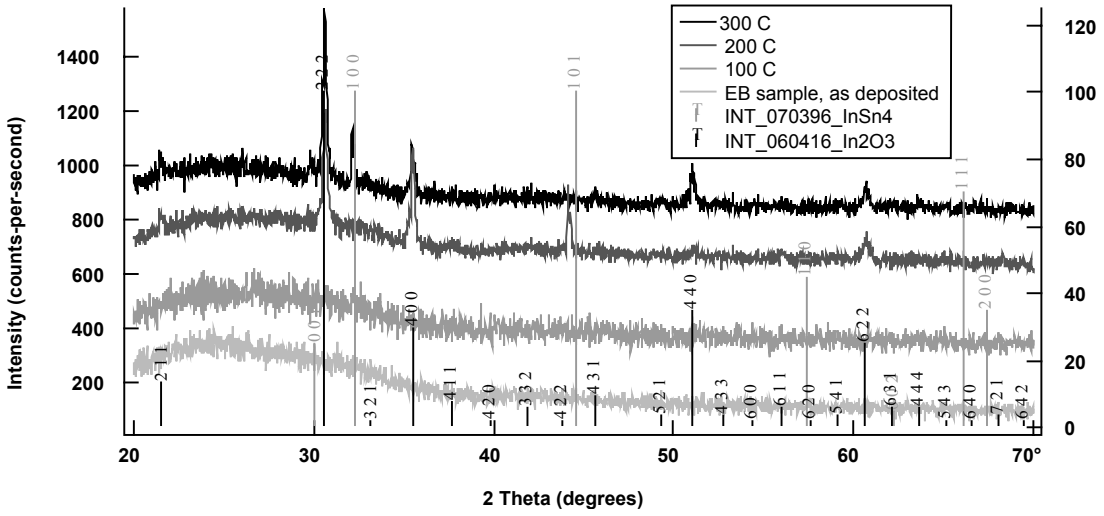

Figure 4 above. Shows x-ray diffraction data for scans of sample EB N-1 (Room Temperature, electron beam deposited) after annealing in increments of 100° C. PDF traces are 7-396 ($InSn_4$) and 6-416 (In_2O_3).

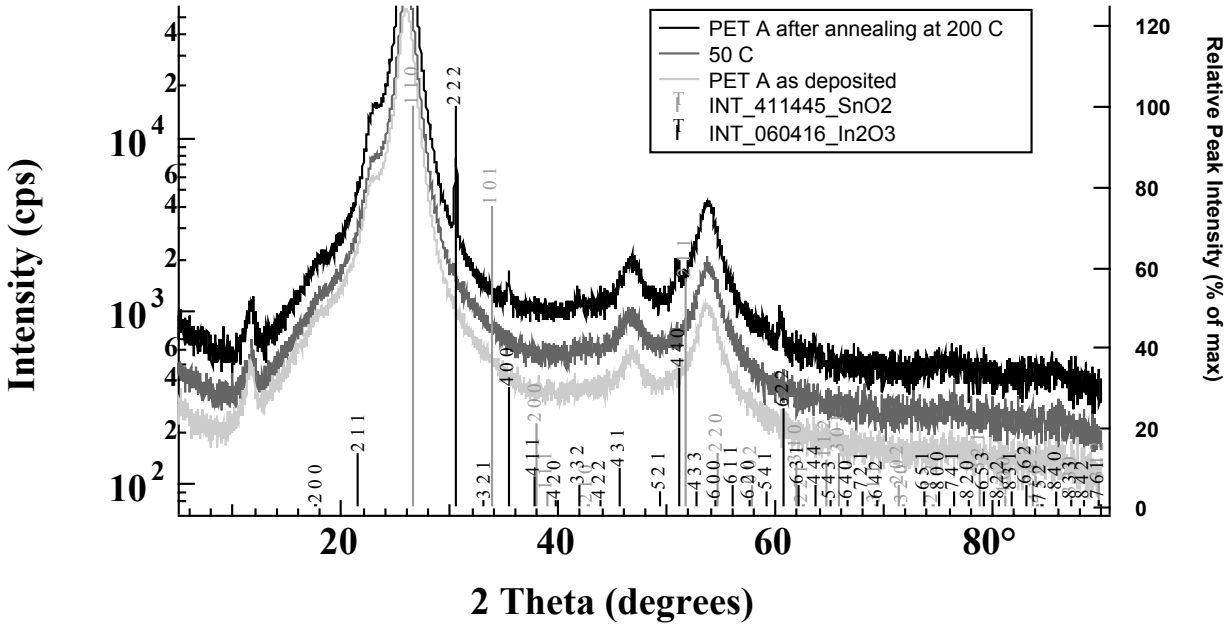

Figure 5 above. PET A XRD scans. PDF traces are 7-396 ($InSn_4$) and 6-416 (In_2O_3).

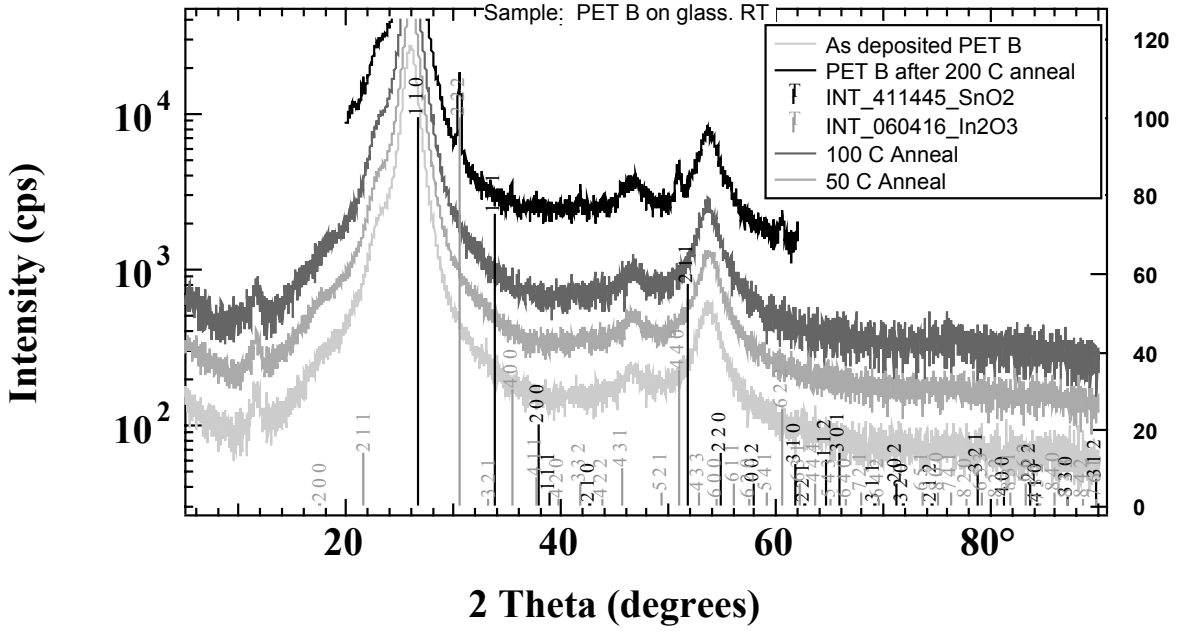

Figure 6 above. PET B XRD scans. Scan after 200 C anneal was taken over a shorter range. PDF traces are 7-396 ($InSn_4$) and 6-416 (In_2O_3).

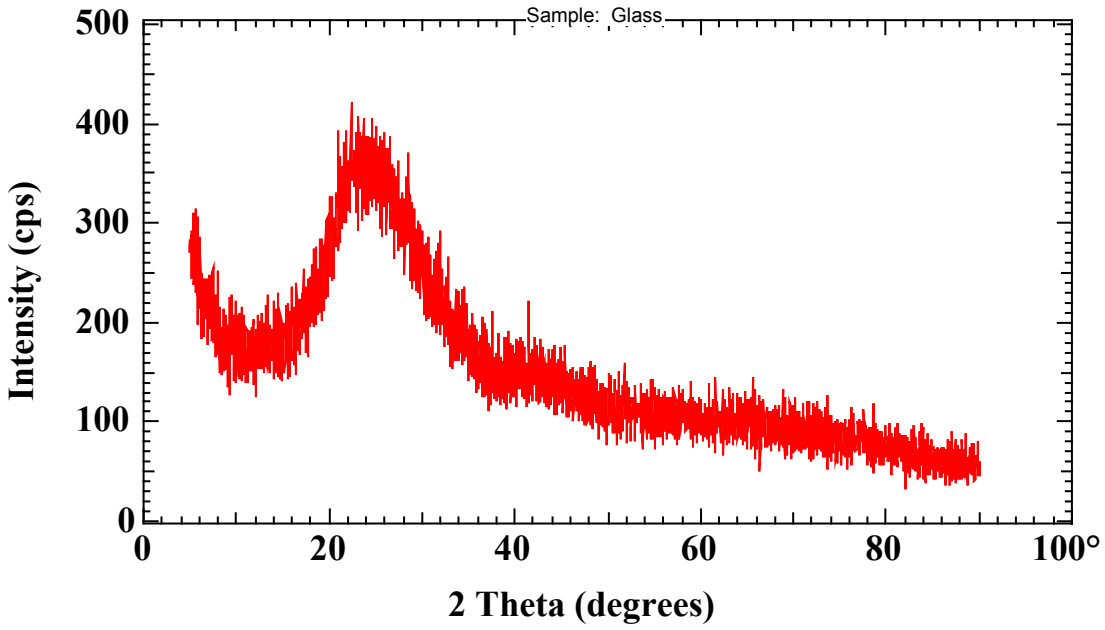

Figure 7 above. XRD scan of the glass substrate. Without any annealing.

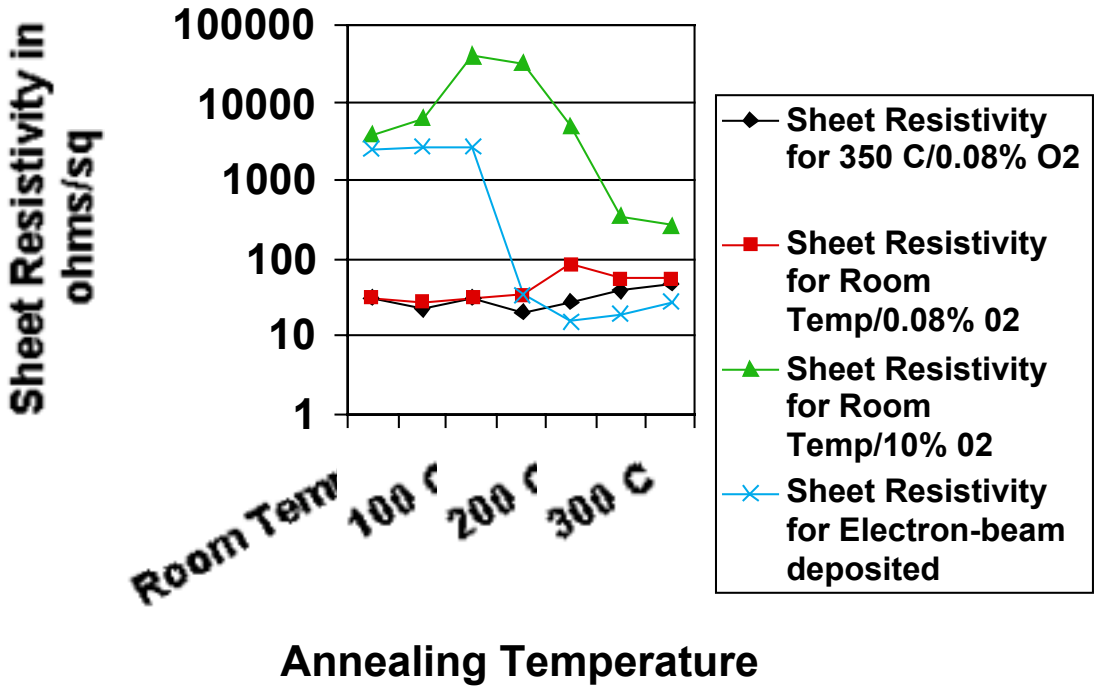

Figure 8 above. Sheet resistivity as a function of annealing temperature.

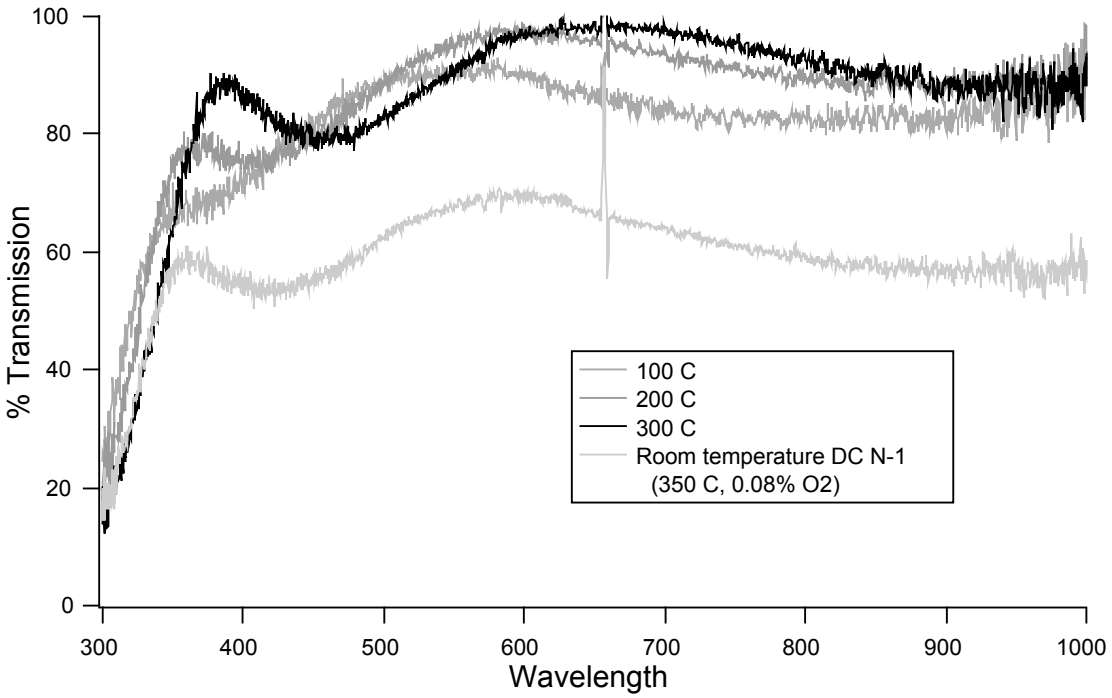

Figure 9 above. Transparency for DC N-1 (350° C/0.08% O2) after annealing in increments of 50° C. Data displayed in 100° C increments.

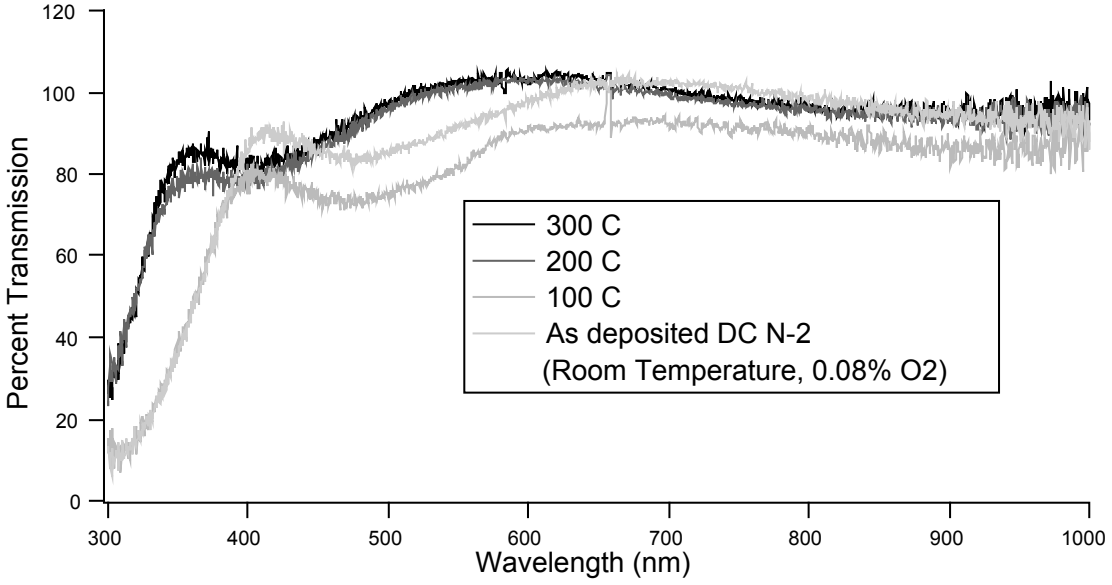

Figure 10 above. Transparency for DC N-2 (Room Temperature/0.08% O2) after annealing in increments of 50° C. Data displayed in 100° C increments.

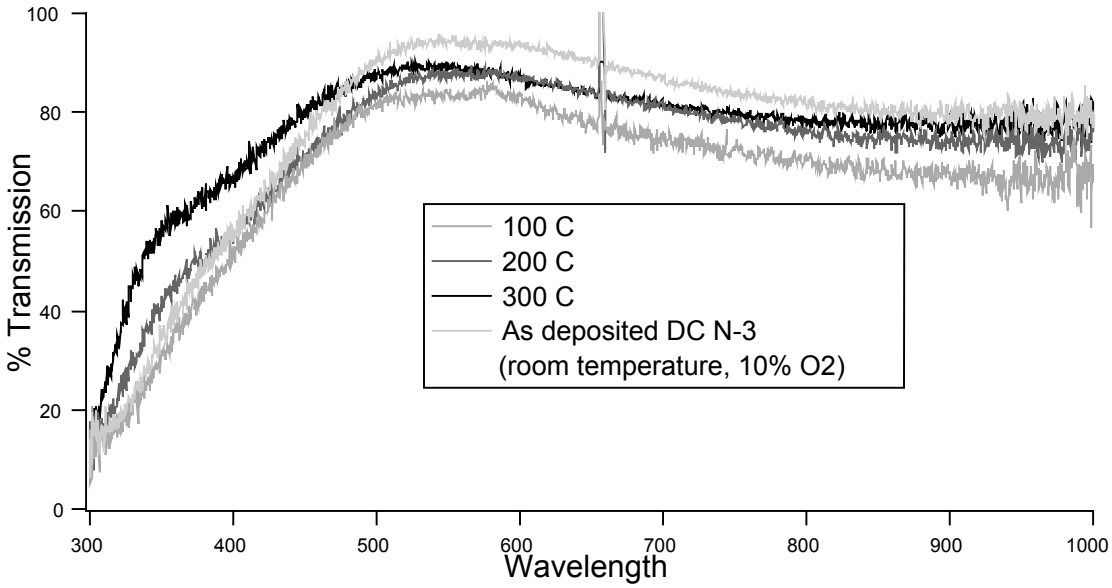

Figure 11 above. Transparency for DC N-3 (Room Temperature/10% O2) after annealing in increments of 50° C. Data displayed in 100° C increments.

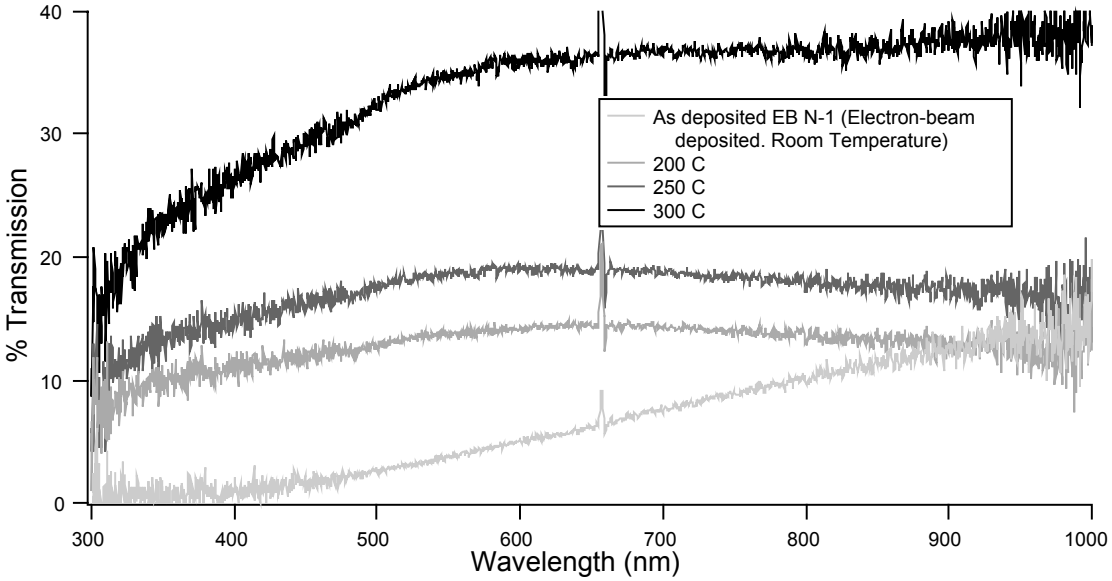

Figure 12 above. Transparency for EB N-1 (Electron-Beam Deposited, Room Temperature) after annealing in increments of 50° C. Data from 50° C, 100° C, and 150° C are not shown because they are the same as the as-deposited data.

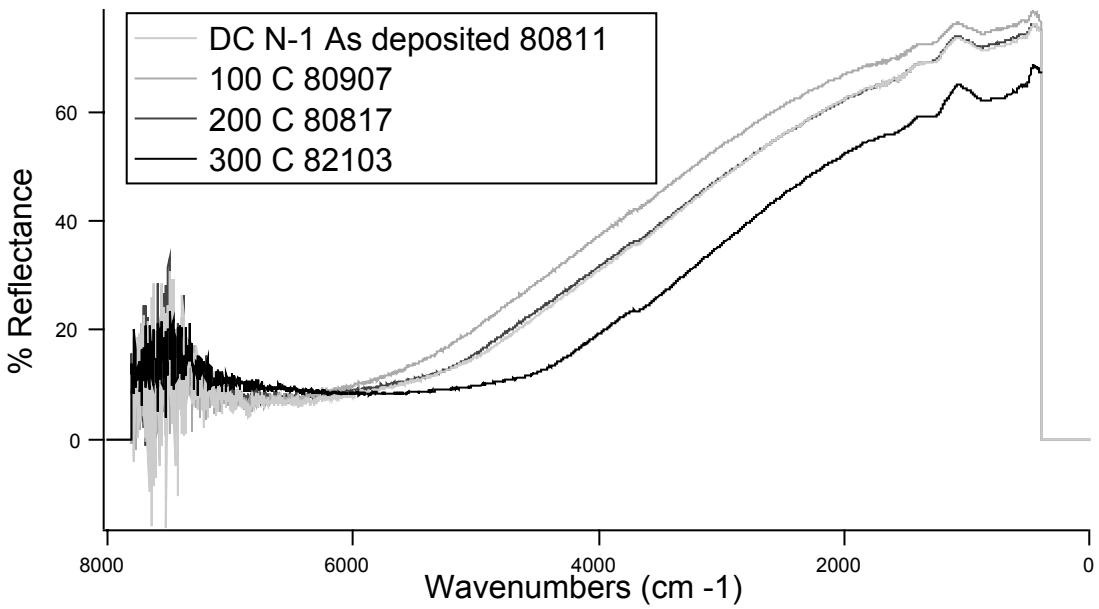

Figure 13 above. FTIR reflectance data for DC N-1 (350° C/ 0.08% O_2). Data taken in 50° C increments and displayed in 100° C increments.

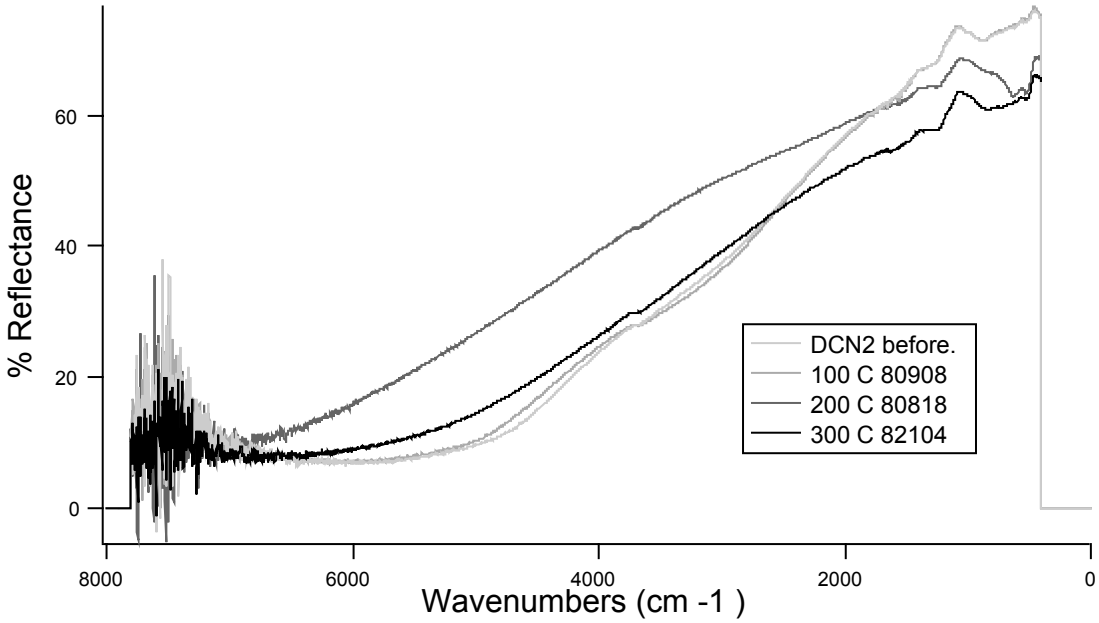

Figure 14 above. FTIR reflectance data for DC N-2 (Room Temperature/ 0.08% O_2). Data taken in 50° C increments and displayed in 100° C increments.

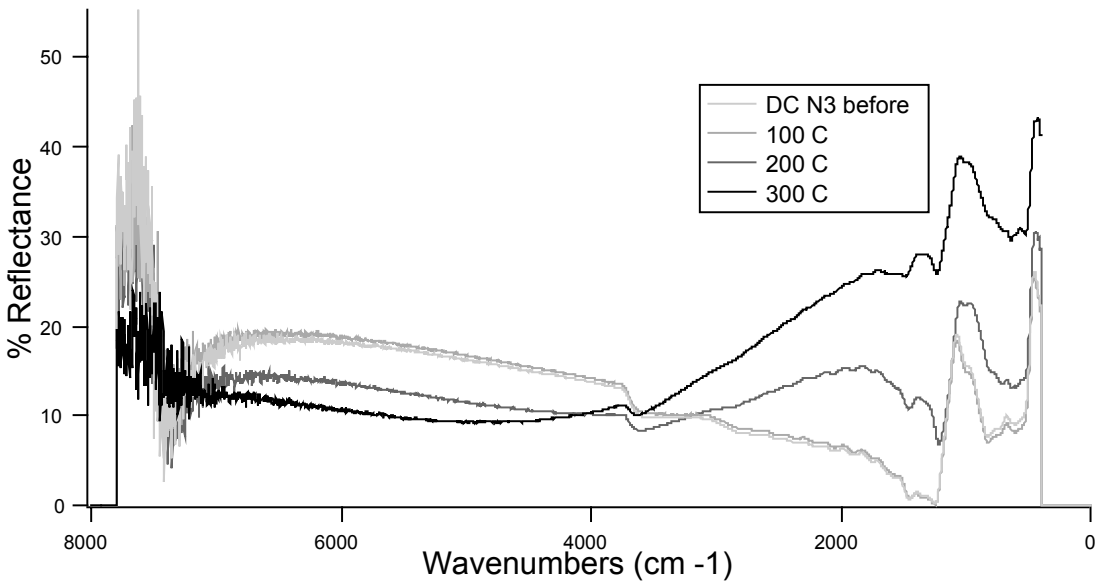

Figure 15 above. FTIR reflectance data for DC N-3 (Room Temperature/ 10% O_2). Data taken in 50° C increments and displayed in 100° C increments.

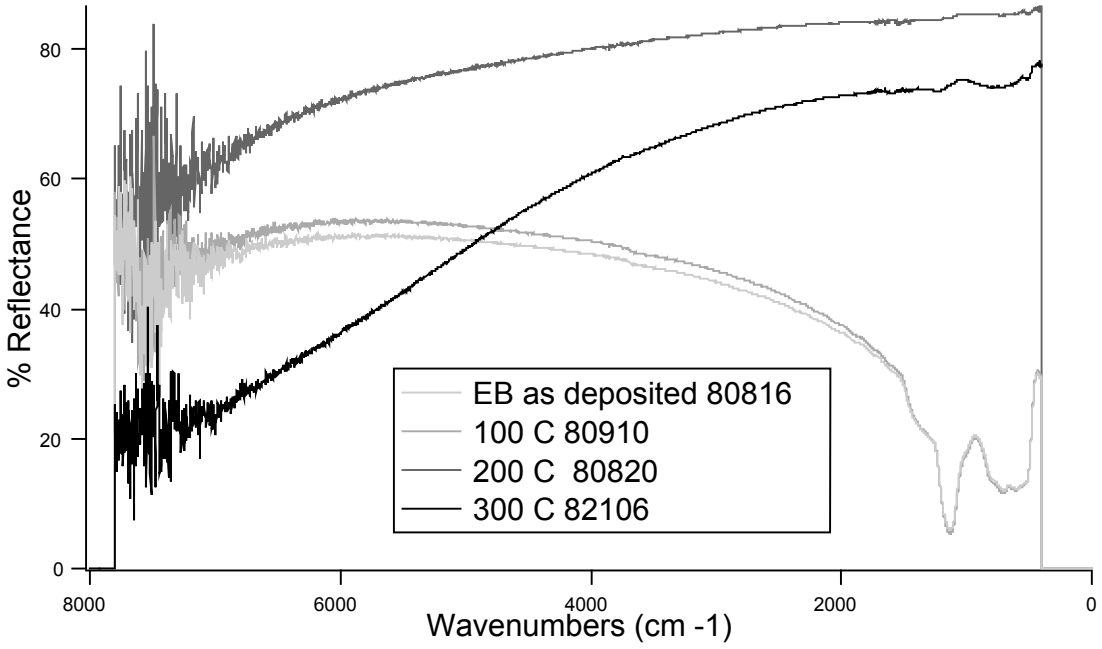

Figure 16 above. FTIR reflectance data for EB N-1 (Electron Beam Deposited, Room Temperature). Data taken in 50° C increments and displayed in 100° C increments.

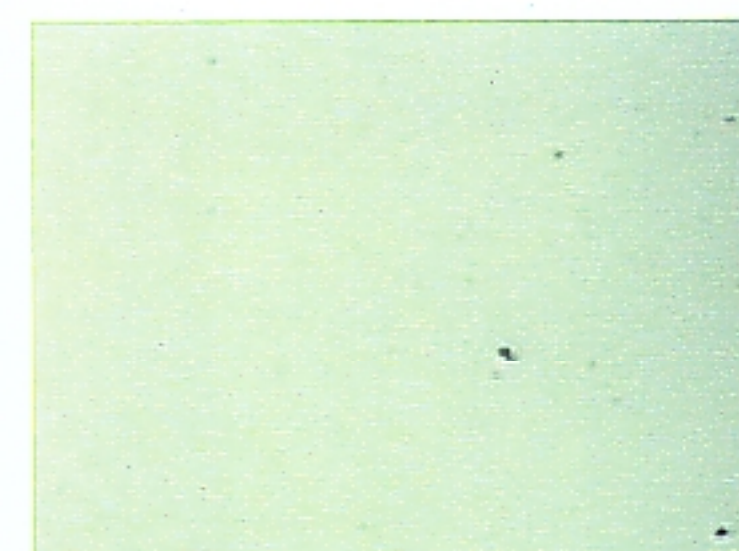

Figure 17 above. Photograph of unannealed electron-beam deposited sample viewed with a compound light microscope at 1000x magnification.

Figure 18 above. Photograph of electron-beam deposited sample annealed at 200° C viewed with a compound light microscope at 1000x magnification.

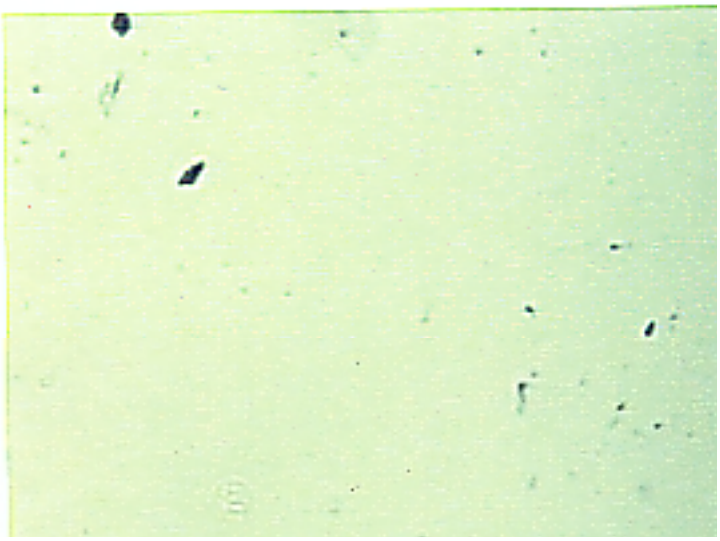

Figure 19 above. Photograph of unannealed electron-beam deposited sample viewed with a compound light microscope at 50x magnification.

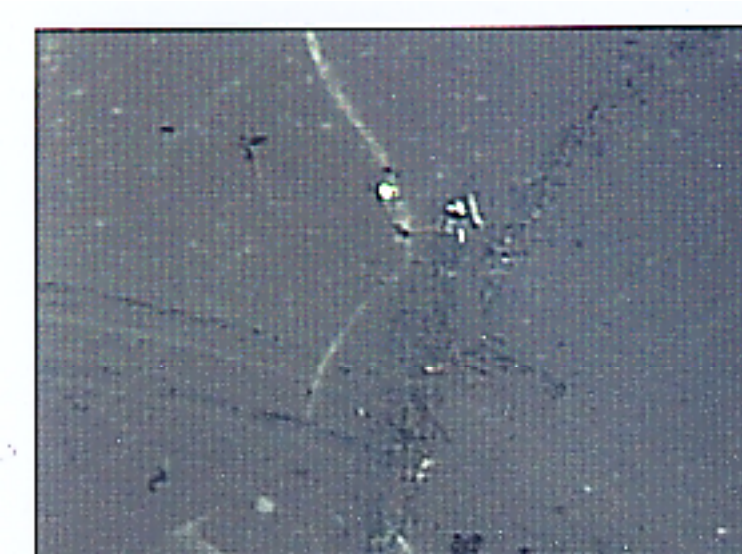

Figure 20 above. Photograph of electron-beam deposited sample annealed at 200°C viewed with a compound light microscope at 1000x magnification.